Entanglement of two nitrogen-vacancy ensembles via a nanotube

Yong-Hong Ma,[1] Quan-Zhen Ding,[2] and E Wu[1,*]

[1]*School of Science, Inner Mongolia University of Science and Technology, Baotou 014010, People's Republic of China*

[2]*Center for Controlled Quantum Systems and Department of Physics and Engineering Physics, Stevens Institute of Technology, Hoboken, New Jersey 07030, USA*

(Received 2 September 2019; accepted 13 January 2020; published 10 February 2020)

As an essential quantum resource in quantum information processing, entanglement between macroscopic systems has been applied to both quantum technologies and foundational studies of the boundary between the quantum and classical worlds. Inspired by the proposal by Li *et al.* [Phys. Rev. Lett. **117**, 015502 (2016)], we propose a scheme that is composed of two separated nitrogen-vacancy centers coupled to the vibration mode of a nanotube for creating entanglement between the two ensembles. An approximate analytical solution related to the calculation of macroscopic entanglement for this two-spin-ensemble model is derived. This kind of analytical solution will be crucial for directly testing the contribution of the experimental parameters, especially for the calculation of macroscopic entanglement in follow-up work. Including the dephasing and mechanical dissipation, we show that two spin ensembles are entangled with time evolution under realistic experimental conditions. This macroscopic entanglement is applicable for applied ideas related to quantum computation and communication, as well as the studies of the boundary between quantum and classical worlds. Moreover, we describe how to realize this practical model and demonstrate this macroscopic entanglement in experiments.

DOI: 10.1103/PhysRevA.101.022311

I. INTRODUCTION

Entanglement is the most prominent and distinctive feature of quantum mechanics [1], as it plays an important role in both tests of fundamental quantum mechanics and applications in the field of quantum technology, including quantum computers, long-distance quantum cryptography, and the increase of sensitivity in quantum metrology [2–4]. In earlier research it was generally believed that quantum entanglement existed in microscopic systems consisting of few particles. Whether quantum entanglement can exist in macroscopic systems has been at the heart of foundational debates [5–7]. In the past decade, there has been an explosion of interest in entanglement in macroscopic (many-body) physical systems [8]. Studying macroscopic entanglement is an effective way to probe the quantum-to-classical transition. At present, a number of different theoretical and experimental methods to create entanglement at the macroscopic level have been achieved. Macroscopic entanglement has been theoretically demonstrated [9] and experimentally generated [10,11] between atomic ensembles.

Macroscopic entanglement can also be created in solid-state systems. It is vital for the storage and processing of quantum information since electron spins in solid-state systems have long relaxation times [12], high controllability, more storage, and high ability to transfer quantum information [13]. There have been a number of experimental demonstrations of macroscopic entanglement, such as entanglement between superconducting circuits [14,15], nuclei and electrons, and nuclear spin qubits [4,16,17]. Negatively charged nitrogen-vacancy (NV) defect centers in diamonds are particularly interesting solid-state spin qubit systems [18–21] since they can be naturally obtained in bulk diamonds or diamond nanocrystals. The most significant advantage of such systems is that quantum states of an NV center can be coherently manipulated and read out even at room temperature [22–30]. Moreover, no cooling is needed to create a pure initial state that is required for entanglement generation. Ultrafast optical technology has been used to generate and measure an entangled state before any environmental coupling might destroy it [31]. At present, coherent coupling and entanglement between an NV center and nuclear spins of nitrogen [32,33] and carbon-13 [16,34] have also been experimentally demonstrated. However, the research of macroscopic entanglement between NV-center ensembles is still relatively limited. Thus, it is important to design an experimental scheme to generate the macroscopic entanglement between NV-center ensembles.

In this paper, inspired by the ideas proposed in Ref. [35], we consider a hybrid quantum system that consists of two spin ensembles and a nanotube. Each spin ensemble is realized by means of NV centers in a diamond crystal. The biggest advantage of this NV-nanotube coupling is the intrinsic nature of the coupling. On the basis of appropriate experimental parameters, numerical results show that entanglement between two macroscopic spin systems can be generated in this system. Compared with previous work, our scheme has the following character. First, the physics of the dissipation mechanism and spin relaxation, which may play a critical role in practical experiments, are included. Results show that spin dephasing and relaxation can be largely suppressed and accordingly, substantial entanglement can be generated under realistic experimental conditions. Second, we consider the design and control of generating macroscopic entanglement for a realistic

*towue@163.com

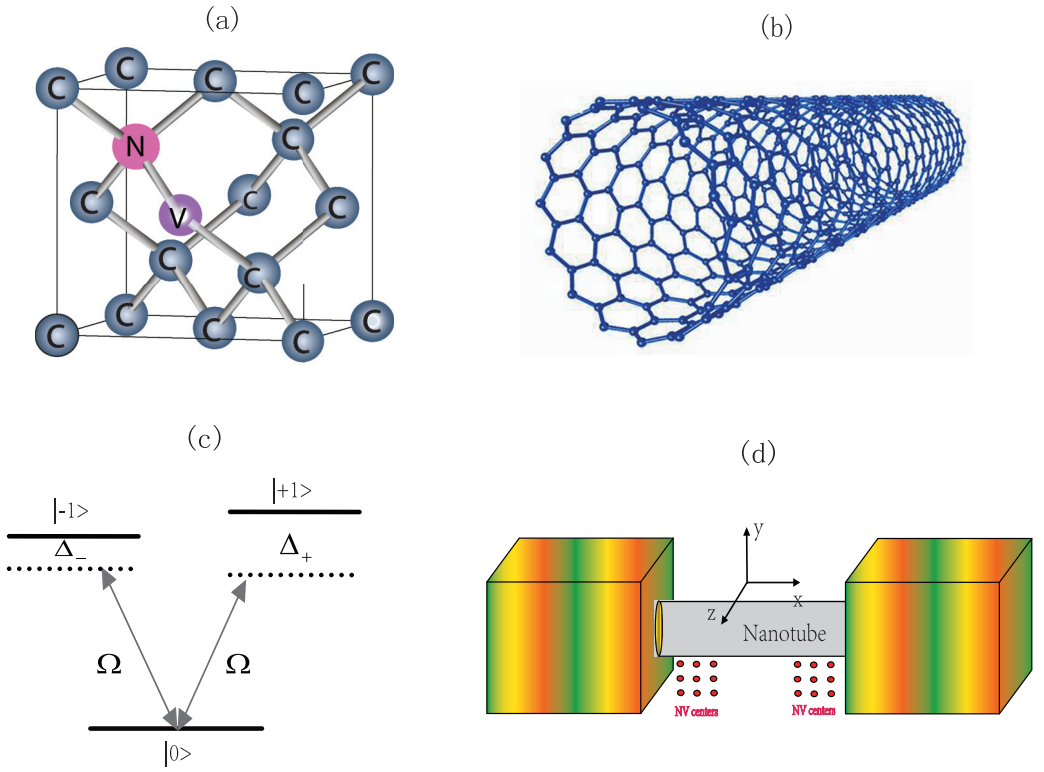

FIG. 1. (a) Structure of a single NV center, which consists of a substitutional nitrogen (N) and a neighboring vacancy (V). (b) Single-walled carbon nanotube, which can be viewed as a graphene sheet that has been rolled up and sewn together. (c) Spin triplet states of the NV electronic ground state driven by two external microwave fields with the same frequency Ω. (d) Schematic diagram of the proposed hybrid quantum system consisting of two NV-center ensembles and a nanotube. Two NV-center ensembles are coupled through a nanotube. The qubit loop is on the y-z plane and perpendicular to the x direction.

setup. It may provide a pathway for experimental realization. More importantly, the analytical solution of the entanglement for this two-spin-ensemble model is derived. This kind of analytical solution may play a very crucial role in calculating the macroscopic entanglement and checking the contribution of experimental parameters.

This paper is organized as follows. In Sec. II we present the model and derive the system Hamiltonian. Including spontaneous emission and spin relaxation of this model, we give the expression of the master equation. The approximate analytical solution and the exact numerical testing of the entanglement for the two-spin-ensemble model is provided in Sec. III. We discuss the main experimental parameters used in our paper in Sec. IV. We describe how to realize this practical experiment and then discuss future research in Sec. V. A summary is given in Sec. VI.

II. MODEL AND HAMILTONIAN

As is shown in Fig. 1, we consider a scheme that is composed of two separated NV centers coupled to the same vibration mode of a nanotube in the dispersive regime. Each NV-center ensemble is placed near a carbon nanotube and composed of N identical and noninteracting NV centers. The magnetomechanical interaction can be engineered and dynamically tuned by external control of the driving microwave fields and electric current through the nanotube. It has been proved that this kind of coupling strength can be about three orders of magnitude stronger than that for cold atoms coupled to nanowires [36]. To achieve the coupling of two NV-center ensembles and spin-nanomechanical hybrid structures effectively, we embed a nanotube between them. The nanotube, which carries a DC, is suspended along the x axis. The motion of the diamond nanoresonator changes the local strain at the position of the NV center, which results in an effective strain-induced electric field [37,38]. We assume that transverse displacement is along the y direction; thus it can be expressed as the fundamental oscillating mode $\hat{E}_y = (\hbar/2m\omega_{\rm nt})^{1/2}(\hat{a}+\hat{a}^{\dagger})$, where $\hat{a}$ is an annihilation operator of the oscillating mode, m is the effective mass of nanotube, and $\omega_{\rm nt}$ is the mechanical vibration frequency [35].

Spin-1 triplet sublevels of the electronic ground state of each NV center with $m_{\rm s}=0$ and $m_{\rm s}=\pm1$ has a zero-field splitting of $D=2.87\,$GHz [38]. We assume that the crystal of the NV center is along the z axis. Two external microwave fields with magnetic field $\vec{B}_{\rm dr}$ drive Rabi oscillations between $|m_s=0\rangle$ and $|m_s=\pm1\rangle$, as shown in Fig. 1(c). We can calculate the magnetic field $\vec{B}_{\rm nt}(\vec{r})$ of the current-carrying nanotube at position $\vec{r}$ by the Biot-Savart law. For a long nanotube, the magnetic field satisfies $\vec{B}_{\rm nt}(\vec{r})=\mu_0 I\vec{e}_x\times\vec{r}/2\pi|\vec{r}|^2$. Here $\vec{e}_x$ is the unit vector in the x direction and I is the electric current in the nanotube. The interaction of a single NV center located at $\vec{r}$ with the total magnetic field is [35,38]

$$\hat{H}_{\rm NV}=\hbar D\hat{S}_z^2+\mu_B g_s B_z\hat{S}_z+\mu_B g_s[\vec{B}_{\rm nt}(\vec{r})+\vec{B}_{\rm dr}]\cdot\hat{\mathbf{S}}, \quad (1)$$

where μ_B is the Bohr magneton, $g_s = 2$ is the Landé factor of the NV center, and $\hat{\mathbf{S}}$ denotes the spin operators of the NV center. By expanding $\vec{B}_{\rm nt}(\vec{r})$ up to first order in $\hat{u}_y$, we obtain

$$\hat{H}_{\rm NV} = \hbar D\hat{S}_z^2 + \mu_B g_s[B_z + B_{\rm nt}(d)]\hat{S}_z + \mu_B g_s \vec{B}_{\rm dr}\cdot\hat{\vec{S}} + \mu_B g_s \hat{S}_z \partial_y B_{\rm nt}\hat{u}_y. \tag{2}$$

According to $\hat{S}_z|m_s\rangle = m_s|m_s\rangle$ ($m_s = 0, \pm 1$), the Hamiltonian can be rewritten in the basis $\hat{S}_z$ as

$$\begin{aligned}\hat{H}_{\rm NV} = &\sum_{m_s}\left\{\langle m_s|\left[\hbar D\hat{S}_z^2 + \mu_B g_s[B_z + B_{\rm nt}(d)]\hat{S}_z\right]|m_s\rangle\right\}|m_s\rangle\langle m_s| + \sum_{m_s,m_s'}\{\langle m_s|\mu_B g_s\vec{B}_{\rm dr}\cdot\hat{\vec{S}}|m_s'\rangle\}|m_s\rangle\langle m_s'| \\ &+ \sum_{m_s}\{\langle m_s|\mu_B g_s\hat{S}_z\partial_y B_{\rm nt}\hat{u}_y|m_s\rangle\}|m_s\rangle\langle m_s|.\end{aligned} \tag{3}$$

Using $\vec{B}_{\rm dr} = B_0\cos\omega_0 t\,\vec{e}_x = B_0/2(e^{i\omega_0 t} + e^{-i\omega_0 t})\vec{e}_x$, we obtain

$$\begin{aligned}\hat{H}_{\rm NV} = &\sum_{m_s}\left\{\hbar D m_s^2 + \mu_B g_s[B_z + B_{\rm nt}(d)]m_s\right\}|m_s\rangle\langle m_s| + \sum_{m_s,m_s'}\frac{1}{2}\mu_B g_s B_0(e^{i\omega_0 t} + e^{-i\omega_0 t})\langle m_s|\hat{S}_x|m_s'\rangle|m_s\rangle\langle m_s'| \\ &+ \sum_{m_s}\mu_B g_s(\hbar/2m\omega_{\rm nt})^{1/2}\partial_y B_{\rm nt} m_s|m_s\rangle\langle m_s|(\hat{a}^\dagger + \hat{a}).\end{aligned} \tag{4}$$

Under the rotating-wave approximation and in the rotating frame ω_0, the above Hamiltonian is derived as

$$\begin{aligned}\hat{H}_{\rm NV} = &(\hbar D + \mu_B g_s B_z + B_{\rm nt} - \hbar\omega_0)|+1\rangle\langle+1| + (\hbar D - \mu_B g_s B_z - B_{\rm nt} - \hbar\omega_0)|-1\rangle\langle-1| \\ &+ \frac{\sqrt{2}}{4}\mu_B g_s B_0(|0\rangle\langle+1| + |+1\rangle\langle 0|) + \frac{\sqrt{2}}{4}\mu_B g_s B_0(|0\rangle\langle-1| + |-1\rangle\langle 0|) \\ &+ \mu_B g_s(\hbar/2m\omega_{\rm nt})^{1/2}\partial_y B_{\rm nt}(|+1\rangle\langle+1| - |-1\rangle\langle-1|)(\hat{a}^\dagger + \hat{a}).\end{aligned} \tag{5}$$

Including the free Hamiltonian of vibration mode, for a single NV center, the Hamiltonian can be expressed as

$$\begin{aligned}\hat{H}_{\rm NV} = &\hbar\omega_{\rm nt}\hat{a}^\dagger\hat{a} + \hbar\Delta_+|+1\rangle\langle+1| + \hbar\Delta_-|-1\rangle\langle-1| \\ &+\hbar\Omega[|-1\rangle\langle 0| + |0\rangle\langle-1|] + \hbar\Omega[|+1\rangle\langle 0| + |0\rangle\langle+1|] \\ &+\hbar g(|+1\rangle\langle+1| - |-1\rangle\langle-1|)(\hat{a}^\dagger + \hat{a}),\end{aligned} \tag{6}$$

with $\hbar\Delta_\pm = \hbar D \pm \mu_B g_s(B_z + B_{\rm nt}) - \hbar\omega_0$, $\hbar\Omega = \frac{\sqrt{2}}{4}\mu_B g_s B_0$, and $\hbar g = \mu_B g_s(\hbar/2m\omega_{\rm nt})^{1/2}\partial_y B_{\rm nt}$. For simplicity, we assume symmetric detunings $\Delta_+ = \Delta_- = \Delta$ and define bright and dark states for NV-center states as

$$\begin{aligned}|B\rangle &= \frac{1}{\sqrt{2}}(|+1\rangle + |-1\rangle), \\ |D\rangle &= \frac{1}{\sqrt{2}}(|+1\rangle - |-1\rangle).\end{aligned} \tag{7}$$

In the dressed state basis $\{|G\rangle = \cos\theta|0\rangle - \sin\theta|B\rangle, |E\rangle = \cos\theta|B\rangle + \sin\theta|0\rangle\}$, with $\tan 2\theta = 2\sqrt{2}\Omega/\Delta$, the Hamiltonian (6) can be reexpressed as [35]

$$\begin{aligned}\hat{H}_{\rm NV} = &\hbar\omega_{\rm nt}\hat{a}^\dagger\hat{a} + \hbar\omega_{eg}|E\rangle\langle E| + \hbar\omega_{dg}|D\rangle\langle D| \\ &+\hbar(g_1|G\rangle\langle D| + g_2|D\rangle\langle E| + \text{H.c.})(\hat{a}^\dagger + \hat{a}),\end{aligned} \tag{8}$$

where the coefficients are $\omega_{eg} = \sqrt{\Delta^2 + 8\Omega^2}$, $\omega_{dg} = \frac{\Delta + \sqrt{\Delta^2 + 8\Omega^2}}{2}$, $g_1 = -g\sin\theta$, and $g_2 = g\cos\theta$. Under a large detuning condition $\Delta \gg \Omega$, we obtain $\sin\theta \simeq 0$, $\cos\theta \simeq 1$, $\omega_{eg} \simeq \Delta + \frac{4\Omega^2}{\Delta}$, $\omega_{dg} \simeq \Delta + \frac{2\Omega^2}{\Delta}$, and $|E\rangle \simeq |B\rangle$, which leads to a simple form

$$\hat{\mathcal{H}}_q = \hbar\omega_{\rm nt}\hat{a}^\dagger\hat{a} + \tfrac{1}{2}\hbar\Lambda\hat{\sigma}_z + \hbar g(\hat{\sigma}_+ + \hat{\sigma}_-)(\hat{a}^\dagger + \hat{a}). \tag{9}$$

After neglecting particle interaction, the Hamiltonian of our system can be expressed as

$$\hat{\mathcal{H}}_q = \hbar\omega_{\rm nt}\hat{a}^\dagger\hat{a} + \frac{1}{2}\hbar\Lambda\sum_{i=1}^{N}\hat{\sigma}_z^i + \hbar g\sum_{i=1}^{N}(\hat{\sigma}_+^i + \hat{\sigma}_-^i)(\hat{a}^\dagger + \hat{a}). \tag{10}$$

For convenience, we introduce collective spin operators such as $J_z = \frac{1}{2}\sum_n(|B\rangle_n\langle B| - |D\rangle_n\langle D|)$, $J_x = \frac{1}{2}\sum_n(|B\rangle_n\langle D| + |D\rangle_n\langle B|)$, $J_+ = \sum_n|B\rangle_n\langle D|$, and $J_- = \sum_n|D\rangle_n\langle B|$. We assume that two NV-center ensembles are separated by a distance $l = 1$ μm and coupled to the same vibration mode of the nanotube with the Hamiltonian

$$\hat{\mathcal{H}} = \hbar\omega_{\rm nt}\hat{a}^\dagger\hat{a} + \frac{1}{2}\hbar\Lambda\sum_{i=1}^{2}J_{iz} + \hbar g\sum_{i=1}^{2}(J_{i+} + J_{i-})(\hat{a}^\dagger + \hat{a}). \tag{11}$$

In the rotating-wave approximation, by using a Schrieffer-Wolff transformation $R = A_0(aJ_{1+} - a^\dagger J_{1-} + aJ_{2-} - a^\dagger J_{2+})$, with $A_0 = \frac{g}{\Lambda - \omega_{\rm nt}}$ for the above Hamiltonian, we obtain

$$\begin{aligned}\hat{\mathcal{H}}_{\rm eff} = &\hbar\omega_{\rm nt}\hat{a}^\dagger\hat{a} + A(J_{1z} + J_{2z}) + B\sum_{j=1}^{2}\left[J_{j+}^2 + J_{j-}^2 + 2J_{j+}J_{j-}\right] \\ &+2B[J_{1+}J_{2+} + J_{1-}J_{2-} + 4(J_{1+}J_{2-} + J_{1-}J_{2+})],\end{aligned} \tag{12}$$

where $A = \frac{1}{2}\Lambda - A_0 g$ and $B = \frac{A_0 g}{2}$. Each NV spin exhibits intrinsic decoherence in the absence of the mechanical mode. The nature of the longitudinal spin relaxation mechanisms is attributed to its temperature dependence. Individual relaxation (T_1) processes are due to lattice phonons. If the temperature is below 60 K, T_1 can be about 100 s; thus we can ignore it [39].

However, intrinsic single-spin dephasing, which arises from the magnetic noise of NV spins in the diamond lattice, should be considered. When NV spins flip, a reversed interaction with its environment will occur. For the sufficiently quick flipping procedure, we can eliminate the effects of a slowly evolving environment. Ultimately, this so-called dynamical decoupling technique can extend the spin quantum coherence time to the spin-lattice relaxation time, removing the effects of the surrounding electronic and nuclear spins [40]. In practice, single spin dephasing may be nonexponential [38], but for simplicity we approximate the effect of spin dephasing by an effective Markovian master equation $\rho_{\rm dep}$ with dephasing rate $1/T_2$,

$$\dot{\rho}_{\rm dep} = \frac{1}{T_2}\sum_n \left[\sigma_{nz}\rho\sigma_{nz} - \frac{1}{2}\left(\sigma_{nz}^2\rho + \rho\sigma_{nz}^2\right)\right]. \tag{13}$$

Mechanical dissipation of the nanotube is described by the master equation for the system density matrix ρ_m,

$$\begin{aligned}\dot{\rho}_m = {}& \gamma(n_{th}+1)\left[a\rho a^\dagger - \tfrac{1}{2}(a^\dagger a\rho + \rho a^\dagger a)\right] \\ & + \gamma n_{th}\left[a^\dagger\rho a - \tfrac{1}{2}(aa^\dagger\rho + \rho aa^\dagger)\right],\end{aligned} \tag{14}$$

where $n_{th} = \frac{1}{e^{\hbar\omega_{\rm nt}/\kappa_B T}-1}$ is the equilibrium phonon occupation number at temperature T. Transforming a and $a^\dagger$ using the transformation $R = A_0(aJ_{1+} - a^\dagger J_{1-} + aJ_{2-} - a^\dagger J_{2+})$, we obtain effective spin relaxation terms in the master equation,

$$\begin{aligned}\dot{\rho}_m = {}& \Gamma(n_{th}+1)\sum_{j=1}^{2}\left[J_{j-}\rho J_{j+} - \frac{1}{2}(J_{j+}J_{j-}\rho + \rho J_{j+}J_{j-})\right] \\ & + \Gamma n_{th}\sum_{j=1}^{2}\left[J_{j+}\rho J_{j-} - \frac{1}{2}(J_{j-}J_{j+}\rho + \rho J_{j-}J_{j+})\right],\end{aligned} \tag{15}$$

where $\Gamma = \frac{g^2\gamma}{(\Lambda-\omega_{\rm nt})^2}$ is the effective dissipative rate. Including spontaneous emission and spin relaxation of this model with Eqs. (13) and (15), the master equation for the density matrix ρ can be expressed as

$$\begin{aligned}\dot{\rho} = {}& -i[H_{\rm eff},\rho] + \Gamma(n_{th}+1)\sum_{j=1}^{2}\left[J_{j-}\rho J_{j+}\right. \\ & \left. - \frac{1}{2}(J_{j+}J_{j-}\rho + \rho J_{j+}J_{j-})\right] \\ & + \Gamma n_{th}\sum_{j=1}^{2}\left[J_{j+}\rho J_{j-} - \frac{1}{2}(J_{j-}J_{j+}\rho + \rho J_{j-}J_{j+})\right] \\ & + \frac{1}{T_2}\sum_{j=1}^{2}\sum_n\left[\sigma_{njz}\rho\sigma_{njz} - \frac{1}{2}\left(\sigma_{njz}^2\rho + \rho\sigma_{njz}^2\right)\right].\end{aligned} \tag{16}$$

III. ENTANGLEMENT BETWEEN NV-CENTER ENSEMBLES

In this section we numerically investigate macroscopic entanglement between two NV-center ensembles. In the experiment, the quantum variables that are compared to the position and momentum operators are two projections of the collective spin of an NV-center sample. If we initialize the spin-polarized NV samples along the x axis, the analog, which is based on the commutation relation $[J_z, J_y] = iJ_x$, can be written as $[X, P] = i$, with $X = J_z/\sqrt{J_x}$ and $P = J_z/\sqrt{J_y}$. In this way, the collective spins of two samples in our model are correlated in the $\hat{\mathbf{y}}$ and $\hat{\mathbf{z}}$ directions. The amount of entanglement condition translates into the form [41]

$$\xi = \frac{{\rm Var}(J_{y1}+J_{y2}) + {\rm Var}(J_{z1}+J_{z2})}{|\langle J_{x1}\rangle| + |\langle J_{x2}\rangle|}, \tag{17}$$

where ${\rm Var}(\cdots)$ represents the statistical variance. If $\xi < 1$, this system is entangled between two macroscopic spin ensembles. To generate such an entangled state of spin ensembles, we initialize the ensemble 1 in a coherent spin state (CSS) along the x axis and another one in the CSS along $-x$ for ensemble 2 such that $\langle J_{1x}\rangle = J$, $\langle J_{2x}\rangle = -J$, $\langle J_{iy}\rangle = \langle J_{iz}\rangle = \langle C_{iyz}\rangle = 0$, and $\langle J_{iy}^2\rangle = \langle J_{iz}^2\rangle = J/2$ $(i = 1, 2)$. In experimental entanglement of two macroscopic objects, two macroscopic atomic samples have been prepared initially in the CSS [10,11]. Similar to macroscopic atomic ensembles [11], we can prepare the CSS using optical pumping and microwave spin manipulation for NV-center spin ensembles. According to the definition of ξ in Eq. (17), to calculate ξ, we need to solve this linear set of equations (A1)–(A8). The full analytic solutions of these linear equations are exceedingly difficult. However, the approximate solutions for the entanglement parameter can be derived, which agree with exact numerics (dotted or dashed lines in Figs. 2 and 3). Based on the exact results of numerical simulation, the maximum value of entanglement occurs around $JBT = 0.1$. If the conditions $\Gamma n_{th}, T_2^{-1} < JB$ and $JBT < 0.2$ are satisfied, some terms with a near-zero contribution can be neglected. We obtain approximately

$$\xi \approx \frac{J[0.75 + 0.1597\cos(12\sqrt{3+\sqrt{13}}JBt) + 0.0903\cosh(12\sqrt{-3+\sqrt{13}}JBt)] + \Gamma(2n_{th}+1)J^2t}{(J+0.25)e^{[-(\Gamma/2)(2n_{th}+1)-2/T_2]t} + 0.048\,343\,8\cos(12\sqrt{3+\sqrt{13}}JBt) - 0.298\,344\cosh(12\sqrt{-3+\sqrt{13}}JBt)}. \tag{18}$$

Obviously, ξ is not dependent on the coefficient A, which agrees with the effective Hamiltonian (12). This kind of macroscopic entanglement arises from correlated quantum terms $2B[J_{1+}J_{2+} + J_{1-}J_{2-} + 4(J_{1+}J_{2-} + J_{1-}J_{2+})]$ rather than $A(J_{1z} + J_{2z})$.

In the following numerical calculations, the influence of the parameters, such as B, Γ, n_{th}, and N, on ξ is analyzed. We plot Figs. 2 and 3 based on the exact solutions of Eqs. (A1)–(A8) (solid or dash-dotted lines in the figures) and the approximate solution of Eq. (18) (dotted or dashed lines in the figures). The results show that the approximate analytical solutions are in agreement with the exact solutions. In the present system, a nanotube is employed to generate macroscopic entanglement between spin ensembles, where

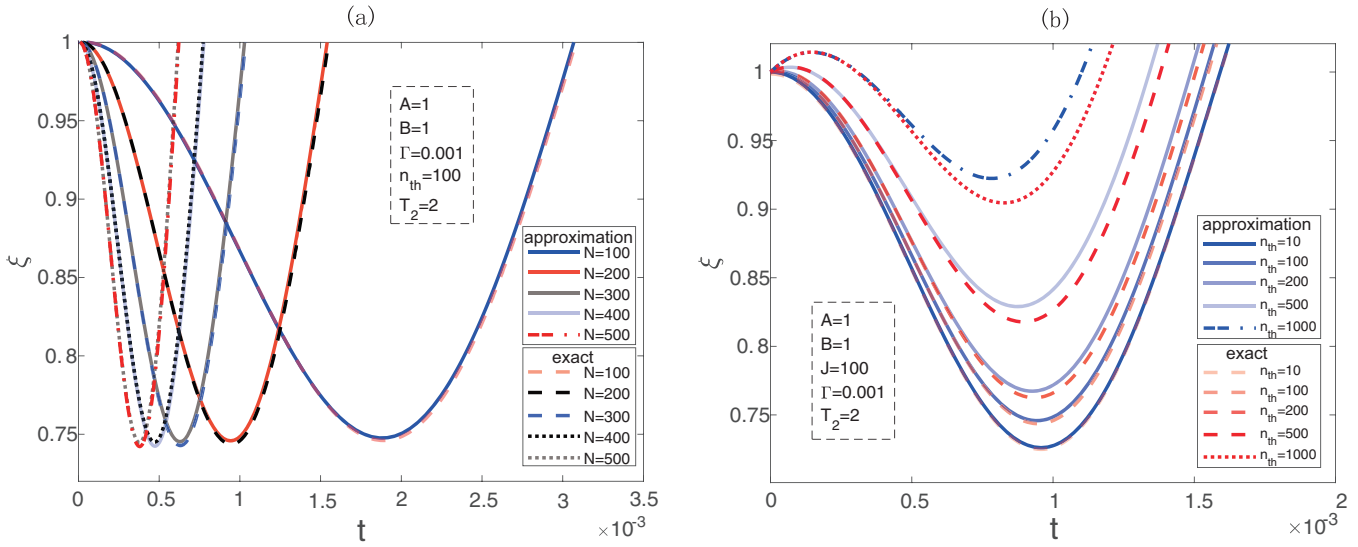

FIG. 2. Entanglement parameter ξ as a function of t with (a) different NV-center numbers and (b) different equilibrium phonon occupation number n_{th}, which is related to the temperature T of the nanotube. Solid (dash-dotted) lines and dashed (dotted) lines show the entanglement calculated using the approximation discussed in the text and the exact numerics, respectively. The relative parameters are $A = 1$, $B = 1$, $\Gamma = 0.001$, $T_2 = 2$, and (a) $n_{th} = 100$ and (b) $J = N/2 = 100$.

the nanotube acts as a common quantum bus. Figure 2(a) shows the evolution of macroscopic entanglement with different NV-center numbers for $\Gamma = 0.001$, which corresponds to a relatively weak dissipation within a finite temperature. We find that the degree of entanglement increases, while the period of the entanglement is reduced, with increasing N. We can explain that a large number of NV centers can cause strong coupling between NV centers via the nanotube. In experiment, the spin number is a more convenient parameter that can be effectively controlled. Thus, a large number of NV centers can quickly generate a maximum macroscopic entanglement. Figure 2(b) shows the entanglement dynamics with the equilibrium phonon occupation number n_{th} at the temperature T. Obviously, relatively small phonon occupation numbers of the nanotube not only can make entanglement appear earlier, but also can increase the maximum entanglement values.

Figure 3(a) shows the entanglement dynamics with different dissipation rates Γ. For $\Gamma = 0.0001$ corresponding to relatively less dissipation to the environment, stronger entanglement with a long period can be generated. The degree of entanglement decreases rapidly with increasing memory parameter Γ. For $\Gamma = 0.01$, which corresponds to a large dissipation and a strong Markovian effect, we can see a very weak entanglement ($\xi = 0.85$) with a very short period. The reason is that, for the Markov case, the environment induces

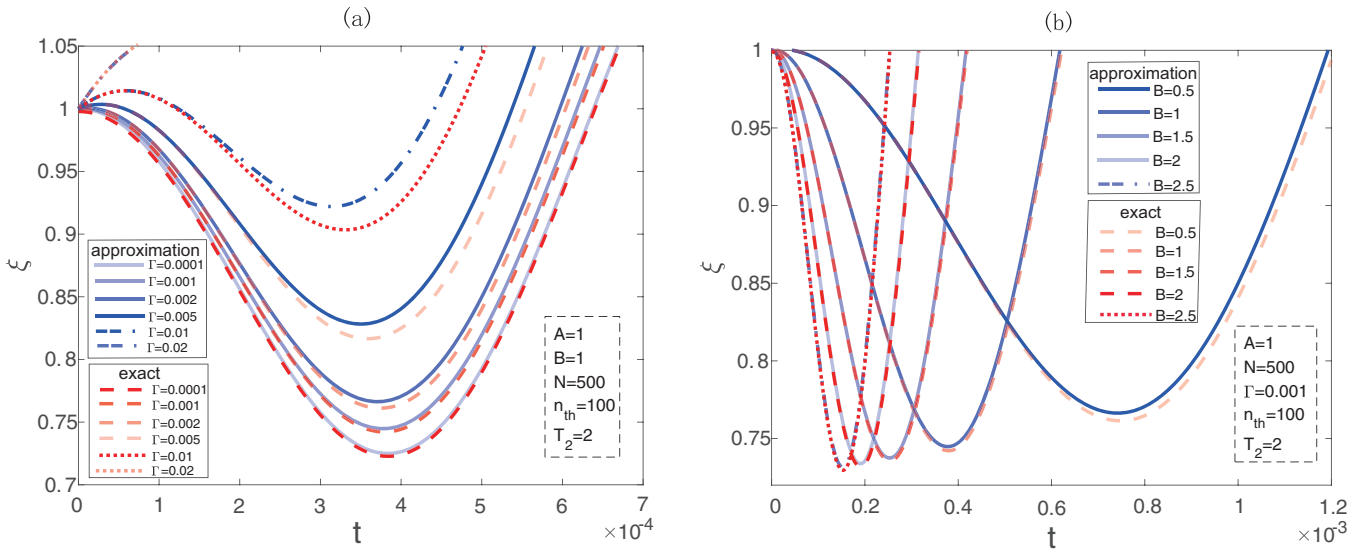

FIG. 3. Entanglement parameter ξ as a function of t with (a) different dissipation rates Γ and (b) different B. Solid (dash-dotted) lines and dashed (dotted) lines show the entanglement calculated using the approximation discussed in the text and the exact numerics, respectively. The relative parameters are $A = 1$, $N = 500$, $n_{th} = 100$, $T_2 = 2$, and (a) $B = 1$ and (b) $\Gamma = 0.001$.

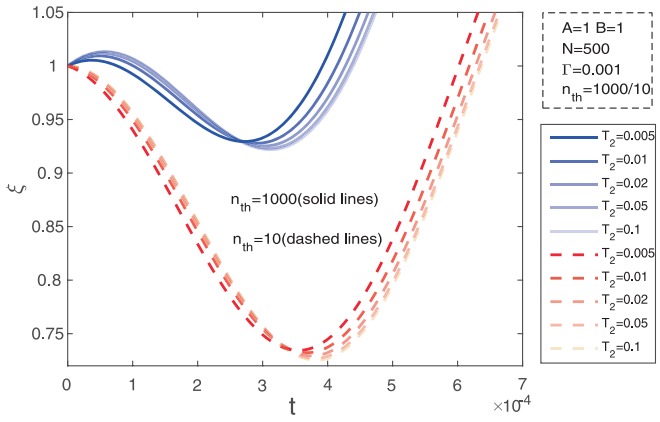

FIG. 4. Entanglement parameter ξ as a function of t with different dephasing times T_2. The relative parameters are $A = 1$, $B = 1$, $N = 500$, $\Gamma = 0.001$, and $n_{th} = 10$ (dashed lines) and $n_{th} = 1000$ (solid lines).

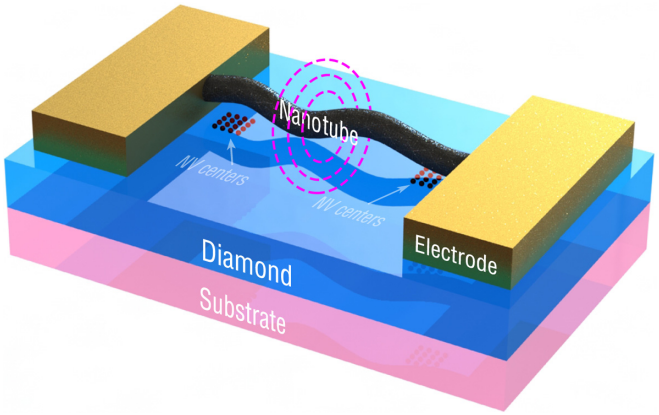

FIG. 5. Experimental device diagram of the proposed hybrid quantum system consisting of two NV-center ensembles and a nanotube.

the system's exponential decay into the environment without an inverse flow of information. Therefore, in order to obtain a strong and long period of macroscopic entanglement, we hope that the dissipative dynamics is weak as long as possible.

Apart from N, Γ, and n_{th}, another important feature of the environment is dictated by the parameter B, which is important in macroscopic entanglement generation. In Fig. 3(b) we plot the evolution of macroscopic entanglement with different parameters B. It is obvious that ξ is less than 1 in a low ratio of B/A from 0.5 to 2.5. As B/A increases, we find that the period of entanglement increases, while the maximum entanglement decreases corresponding to the minimum value of ξ. Moreover, we can see that it takes a long time to create entanglement for a large parameter $B = 0.5$ in Fig. 3(b). Thus, in order to rapidly generate macroscopic entanglement, we choose large values of B. In addition, there is no entanglement when $B \to 0$, which is caused by the disappearance of the nonlinear interaction term $J_{1+}J_{2+} + J_{1-}J_{2-} + 4(J_{1+}J_{2-} + J_{1-}J_{2+})$ that is attributed to the creation of entanglement. For $B = 0$, two levels of spins are almost equally populated, and spins form a standing wave with pronounced interference fringes [42,43]. Hence spins are effectively compressed to half of the volume that would be occupied if they were all circulating in the same direction ($J_z \approx \pm N/2$) without interference fringes [42]. Figure 4 depicts the time evolution of the macroscopic entanglement for the exemplary values $T_2 = [0.005, 0.01, 0.02, 0.05, 0.1]$. It shows that the degree of entanglement slightly increases and then decreases as the dephasing rate $1/T_2$ increases. We also note that the period of the macroscopic entanglement will be slightly reduced with the dephasing rate $1/T_2$ increasing.

IV. SELECTION OF PARAMETERS

In this section we discuss the main parameters $A = \frac{\Omega^2}{\Delta} - \frac{g^2}{\Lambda-\omega_{\rm nt}}$ and $B = \frac{g^2}{2(\Lambda-\omega_{\rm nt})}$ in Eq. (12). By using the Biot-Savart law, the spin-phonon coupling strength g can be written as $g = \frac{\mu_B g_s \mu_0 I}{2\pi\sqrt{2\hbar m\omega_{\rm nt}}d^2}$ [35], which depends on the dimensions of the nanotube, the distance d from the diamond nanocrystal, and the current I flowing through the nanotube. Thus, g can be tuned by controlling the distance d, dimensions of the nanotube, and the current I.

The frequency of the fundamental vibrational mode of a nanotube $\omega_{\rm nt}$ is adjustable, which is expressed as [35] $\omega_{\rm nt} \sim \frac{1}{L^2}\sqrt{\frac{E\mathcal{I}}{\rho M}}$, with L the length of a carbon nanotube, ρ the mass density, M the beam cross section, E the Young modulus, and $\mathcal{I}$ the moment of inertia. Therefore, by changing r and L, $\omega_{\rm nt}$ can be further adjusted. On the basis of the experimental parameters [35] $L = 2\ \mu$m, $r = 1.5$ nm, $\rho = 1.35 \times 10^6$ g/m^3, $m = 7 \times 10^{-21}$ Kg, $I = 60\ \mu$A/nm^2, and $E = 1$ TPa, one can obtain $\omega_{\rm nt} = 4\pi$ MHz and $g/2\pi \sim 10$ kHz. For $d \sim 10$ nm, the magnetomechanical coupling strength can even reach $g/2\pi \sim 100$ kHz [35].

Moreover, the microwave Rabi frequency Ω is also controllable. The Rabi frequency is the frequency of oscillation for a given energy level transition. It also provides the measure of fluctuation of the population between levels. It is associated with the strength of coupling between the light and transition. In all cases, the microwave includes the entire superhigh-frequency band (frequency from 3 to 30 GHz, or wavelength from 10 to 1 cm) at minimum, with Rabi frequency engineering often putting the lower boundary at 1 GHz (30 cm) and the upper around 100 GHz (3 mm). In our system, in the case of resonant coupling of the microwave, the Rabi frequency is equal to the Zeeman splitting, which depends on the amplitude of magnetic fields and is the order of about 1 GHz. We can use the L band (frequency range 1–2 GHz) to couple spin levels $|\pm 1\rangle$ in our system, the frequency of which is less than the frequency of the zero-field splitting (2.88 GHz). By changing the Rabi frequency, the detuning Δ is also adjustable.

V. EXPERIMENTAL REALIZATION AND OUTLOOK

A sketch of the experimental configuration is shown in Fig. 5. A nanotube carrying a DC is suspended above a bulk single-crystal diamond sample. Individual, optically resolvable two-NV-center ensembles are implanted 7–14 nm below the surface of the diamond sample [44]. The carbon nanotube, which is tens of micrometers long, can be deflected

electrostatically over several nanometers with voltages applied to the gate electrodes. In this way, the distance between the nanotube and NV-center ensembles can be varied and fine-tuned by the nanotube's effective transverse displacement. The motion of the nanotube changes the local strain at the position of the NV center. The strength of the band bending in the diamond depends on the density of impurities, which can be varied by the dose of implanted nitrogen [45]. To dynamically manipulate the state of NV centers, a gate voltage is applied between a reference electrode in the electrolyte and the diamond surface. This voltage allows one to electrically shift the Fermi level at the diamond surface, which, at the same time, also changes its surface band bending [45]. The experimental results are based on the NV center existing in the negatively charged NV center. The charge state is determined by the charge transition levels. The fluorescence intensity of the negatively charged NV center is a measure of the ground-state occupation. Therefore, the equilibrium occupation of negatively charged NV transition states is governed exclusively by the position of the Fermi level [46].

Demonstration of macroscopic entanglement has important implications for efforts to realize quantum computation and communication in the near future. In our experimental scheme, entanglement is produced via the interaction of NVs with the oscillating mode of the nanotube. A polarized pulse of the nanotube is described by Stokes operators that obey the same commutation relation as spin operators $[S_y, S_z] = iS_x$, where S_x denotes the difference between phonon numbers of the nanotube in x and y linear polarizations, S_y indicates the difference between polarizations at $\pm 45^\circ$, and S_z is the difference between the left and right circular polarizations along the propagation direction. In our paper, the oscillating mode of the nanotube is linearly polarized along the x axis. Hence the two pairs of continuous quantum variables engaged in the entanglement protocol are J_z and J_y for NVs and S_z and S_y for the nanotube. In order to measure macroscopic entanglement in realistic experiments, we can transfer states from NV centers to states of two additional small nanotubes, each of which is attached to an NV-center ensemble. Thus, the task of entanglement detection can be performed by direct measurement on states of additional nanotubes. Implementation of transferring states from NV-center ensemble to nanotubes could be realized by using a SWAP gate between the jth NV-center ensemble and nanotubes, like the method in [47,48].

We can also extend entanglement between two NV-center ensembles to tripartite or quadripartite macroscopic entanglement. One can generate tripartite macroscopic entanglement by coupling another NV-center ensemble on one side of the NV center based on our model in Fig. 1(a). In this case, numerical calculations become complicated in terms of spin operators used in our calculations. Large-spin approximation and low excitations may be a good way to solve this problem. In these conditions, a bosonic annihilation (creation) operator $a = \frac{1}{\sqrt{N}} \sum_{i=1}^{N} |D\rangle_i\langle B|$ ($a^\dagger = \frac{1}{\sqrt{N}} \sum_{i=1}^{N} |B\rangle_i\langle D|$) is introduced, which satisfies the communication relation $[c, c^\dagger] \simeq 1$ [49,50]. Then we can use multipartite continuous-variable entanglement criteria [51] to calculate this tripartite macroscopic entanglement.

Moreover, the period of macroscopic entanglement for our system may be short for many quantum information applications. This is caused by the room-temperature environment and strong coupling of phonon modes in solids [52]. However, ultrafast optical technology can alleviate experimentally the requirement on quantum coherence time. In the future, with the improvement of ultrafast technology, or by using more isolated degrees of freedom in solids, such as nuclear spins or dopant rare-earth ions, many more quantum operations could be done within the coherence time of solids, even at room temperature [31].

VI. CONCLUSION

Going beyond the early work of Li *et al.* [35], which engineered strong magnetomechanical interactions between a single NV spin and the vibrational mode of the nanotube, we proposed a multiparticle system that consists of two NV-center ensembles in diamond coupled to the vibrational mode of a carbon nanotube. The nanotube with population difference acts as a data bus, which can transfer information between two spin ensembles and the nanotube. Including the spin dephasing and relaxation, we have studied the macroscopical entanglement between two NV-center ensembles. It shows that two spin ensembles are entangled with the help of the nanotube, even in the presence of dephasing and mechanical dissipation. Moreover, we derived the approximate analytical solutions of the entanglement which, in comparison with the exact results of numerical simulation, agree with the approximate analytical solutions. Considering the influence of different experimental parameters on macroscopical entanglement, the simulation results show that entanglement can be controlled by the distance from the diamond nanocrystal, the dimensions of the nanotube, the microwave field, and the current. More importantly, it is an innovation to prove the macroscopic entanglement of two NV-center ensembles and design the experiment scheme. This design and the results may provide a striking example that entanglement not only is generated by microscopic particles but also is created in the macroscopic world. That may open up avenues towards the macroscopic entanglement design of hybrid quantum devices including NV centers. Finally, we have provided a sketch of the experimental configuration that may offer some guidance for future experimental research.

ACKNOWLEDGMENTS

We would like to thank Jia-Han Zhang for helpful discussion. The project was supported by NSFC (Grant No. 11664029) and Distinguished Young Scholars Breeding Fund of Inner Mongolia (Grant No. 2017JQ08).

APPENDIX: EXPECTATION OF COLLECTIVE OPERATORS WITH TIME EVOLUTION

We outline the mean values that enter the variance of Eq. (17). In order to treat the entanglement Hamiltonian, we linearize the equations for the variances. This corresponds to expanding the small error from decoherence at short times.

As is known, for an operator $\hat{O}$, the expectation with time evolution can be expressed by means of the master equation as $d\langle\hat{O}\rangle/dt = \mathrm{tr}[\hat{O}\dot{\rho}]$. Using Eq. (16), we can easily obtain the equations

$$\frac{d\langle J_{jx}\rangle}{dt} = -(A-2B)\langle J_{jy}\rangle + 12B\langle J_{jz}J_{ky}\rangle - \left[\frac{2}{T_2} + \frac{\Gamma}{2}(2n_{th}+1)\right]\langle J_{jx}\rangle + (-1)^{j-1}\Gamma J\langle J_{jz}\rangle, \tag{A1}$$

$$\frac{d\langle J_{jy}\rangle}{dt} = (A-2B)\langle J_{jx}\rangle - 4BJ[2(-1)^{j-1}+5(-1)^{j}]\langle J_{jz}\rangle - \left[\frac{2}{T_2} + \frac{\Gamma}{2}(2n_{th}+1)\right]\langle J_{jy}\rangle + \Gamma n_{th}\langle C_{jyz}\rangle, \tag{A2}$$

$$\frac{d\langle J_{jz}\rangle}{dt} = 4BJ[2(-1)^{j-1}+5(-1)^{j}]\langle J_{jy}\rangle - 12(-1)^{j-1}BJ\langle J_{ky}\rangle - \Gamma(2n_{th}+1)\langle J_{jz}\rangle - \Gamma n_{th}\langle J_{jy}^2\rangle - \Gamma n_{th}J^2, \tag{A3}$$

$$\frac{d\langle J_{jy}^2\rangle}{dt} = 2(-1)^{j-1}(A-2B)J\langle J_{jy}\rangle + 8J[2(-1)^{j-1}-5(-1)^{j}]\langle C_{jyz}\rangle - \left[\frac{2}{T_2} + \frac{\Gamma}{2}(2n_{th}+1)\right]\langle J_{jy}^2\rangle + \Gamma(2n_{th}+1)\langle J_{jz}^2\rangle + \Gamma n_{th}J\langle J_{jz}\rangle - \frac{2}{T_2}J, \tag{A4}$$

$$\frac{d\langle J_{1y}J_{2y}\rangle}{dt} = -(A-2B)J[\langle J_{1y}\rangle - \langle J_{2y}\rangle] - 12JB[\langle J_{1y}J_{2z}\rangle - \langle J_{1z}J_{2y}\rangle] - \Gamma(2n_{th}+1)\langle J_{1y}J_{2y}\rangle + \Gamma n_{th}[\langle C_{1yz}\rangle\langle J_{2y}\rangle + \langle J_{1y}\rangle\langle C_{2yz}\rangle], \tag{A5}$$

$$\frac{d\langle J_{1z}J_{2z}\rangle}{dt} = 12JB[\langle J_{1z}J_{2y}\rangle - \langle J_{1y}J_{2z}\rangle + \langle C_{1yz}\rangle - \langle C_{2yz}\rangle] - 2\Gamma(2n_{th}+1)\langle J_{1z}J_{2z}\rangle - \frac{\Gamma}{2}n_{th}J^2(\langle J_{1z}\rangle + \langle J_{2z}\rangle) - \Gamma n_{th}\left(\langle J_{1y}^2\rangle\langle J_{2z}\rangle + \langle J_{1z}\rangle\langle J_{2y}^2\rangle\right), \tag{A6}$$

$$\frac{d\langle J_{jz}J_{ky}\rangle}{dt} = (-1)^{j}(A-2B)J\langle J_{jz}\rangle + 4BJ[2(-1)^{j-1}+5(-1)^{j}](\langle J_{1y}J_{2y}\rangle + \langle J_{1z}J_{2z}\rangle) - 12(-1)^{j-1}JB\langle J_{ky}^2\rangle - \left[\frac{2}{T_2} + \frac{3\Gamma}{2}(2n_{th}+1)\right]\langle J_{jz}J_{ky}\rangle - \Gamma n_{th}J^2\langle J_{ky}\rangle - \Gamma n_{th}\left(\langle J_{jy}^2\rangle\langle J_{ky}\rangle + \langle J_{jz}\rangle\langle C_{kyz}\rangle\right), \tag{A7}$$

$$\frac{d\langle C_{jyz}\rangle}{dt} = (-1)^{j-1}(A-2B)J\langle J_{jz}\rangle + 4BJ[(-1)^{j-1}+5(-1)^{j}]\left(\langle J_{jy}^2\rangle - \langle J_{jz}^2\rangle\right) - 12(-1)^{j-1}J\langle J_{1y}J_{2y}\rangle - \left[\frac{4}{T_2} + \frac{5\Gamma}{2}(2n_{th}+1)\right]\langle C_{jyz}\rangle - \Gamma n_{th}J^2\langle J_{jy}\rangle, \tag{A8}$$

where we define the covariance operator $\langle C_{jyz}\rangle = \langle J_{jy}J_{jz} + J_{jz}J_{jy}\rangle/2$, with $j,k = 1,2$ $(j \neq k)$. Equations of motion including $\langle J_{jx,kx}\rangle$, $\langle J_{jy,ky}\rangle$, and $\langle J_{jz,kz}\rangle$ provide the first-order (drift) terms in the partial differential equation, while equations of motion for symmetric-ordered operator pairs like $\langle C_{jyz}\rangle$ provide the second-order (diffusion) terms.

[1] R. Horodecki, P. Horodecki, M. Horodecki, and K. Horodecki, Rev. Mod. Phys. **81**, 865 (2009).

[2] S. Mancini, V. Giovannetti, D. Vitali, and P. Tombesi, Phys. Rev. Lett. **88**, 120401 (2002).

[3] S. L. Braunstein and P. van Loock, Rev. Mod. Phys. **77**, 513 (2005).

[4] F. Dolde, I. Jakobi, B. Naydenov, N. Zhao, S. Pezzagna, C. Trautmann, J. Meijer, P. Neumann, F. Jelezko, and J. Wrachtrup, Nat. Phys. **9**, 139 (2013).

[5] A. J. Leggett and A. Garg, Phys. Rev. Lett. **54**, 857 (1985).

[6] L. Diosi, Phys. Rev. A **40**, 1165 (1989).

[7] R. Penrose, Gen. Relat. Gravit. **28**, 581 (1996).

[8] L. Amico, R. Fazio, A. Osterloh, and V. Vedral, Rev. Mod. Phys. **80**, 517 (2008).

[9] C. A. Muschik, E. S. Polzik, and J. I. Cirac, Phys. Rev. A **83**, 052312 (2011).

[10] H. Krauter, C. A. Muschik, K. Jensen, W. Wasilewski, J. M. Petersen, J. I. Cirac, and E. S. Polzik, Phys. Rev. Lett. **107**, 080503 (2011).

[11] B. Julsgaard, A. Kozhekin, and E. S. Polzik, Nature (London) **413**, 400 (2001).

[12] G. Feher, Phys. Rev. **114**, 1219 (1959).

[13] Z. L. Xiang, S. Ashhab, J. Q. You, and F. Nori, Rev. Mod. Phys. **85**, 623 (2013).

[14] E. Rittweger, D. Wildanger, and S. W. Hell, Europhys. Lett. **86**, 14001 (2009).

[15] B. Naydenov, F. Reinhard, A. Lammle, V. Richter, R. Kalish, U. F. S. D'Haenens-Johansson, M. Newton, F. Jelezko, and J. Wrachtrup, Appl. Phys. Lett. **97**, 242511 (2010).

[16] P. Neumann, N. Mizuochi, F. Rempp, P. Hemmer, H. Watanabe, S. Yamasaki, V. Jacques, T. Gaebel, F. Jelezko, and J. Wrachtrup, Science **320**, 1326 (2008).

[17] W. Pfaff, T. H. Taminiau, L. Robledo, H. Bernien, M. Markham, D. J. Twitchen, and R. Hanson, Nat. Phys. **9**, 29 (2012).

[18] I. Aharonovich, A. D. Greentree, and S. Prawer, Nat. Photon. **5**, 397 (2011).

[19] J. L. O'Brien, A. Furusawa, and J. Vuckovic, Nat. Photon. **3**, 687 (2009).

[20] R. Hanson and D. D. Awschalom, Nature (London) **453**, 1043 (2008).
[21] T. D. Ladd, F. Jelezko, R. Laflamme, Y. Nakamura, C. Monroe, and J. L. O'Brien, Nature (London) **464**, 45 (2010).
[22] D. M. Toyli, D. J. Christle, A. Alkauskas, B. B. Buckley, C. G. Van de Walle, and D. D. Awschalom, Phys. Rev. X **2**, 031001 (2012).
[23] J. Wolters, N. Sadzak, A. W. Schell, T. Schröder, and O. Benson, Phys. Rev. Lett. **110**, 027401 (2013).
[24] A. Gruber, A. Dräbenstedt, C. Tietz, L. Fleury, J. Wrachtrup, and C. von Borczyskowski, Science **276**, 2012 (1997)
[25] E. C. Reynhardt and G. L. High, J. Chem. Phys. **109**, 4090 (1998).
[26] F. Jelezko, I. Popa, A. Gruber, and J. Wrachtrup, Appl. Phys. Lett. **81**, 2160 (2002).
[27] J. Köhler, J. A. J. M. Disselhorst, M. C. J. M. Donckers, E. J. J. Groenen, J. Schmidt, and W. E. Moerner, Nature (London) **363**, 242 (1993).
[28] F. Jelezko, T. Gaebel, I. Popa, A. Gruber, and J. Wrachtrup, Phys. Rev. Lett. **92**, 076401 (2004).
[29] P. Siyushev, M. Nesladek, E. Bourgeois, M. Gulka, J. Hruby, T. Yamamoto, M. Trupke, T. Teraji, J. Isoya, and F. Jelezko, Science **363**, 728 (2019).
[30] G. Q. Liu, X. Feng, N. Wang, Q. Li, and R. B. Liu, Nat. Commun. **10**, 1344 (2019).
[31] L. M. Duan, Science **334**, 1213 (2011).
[32] T. Gaebel, M. Domhan, I. Popa, C. Wittmann, P. Neumann, F. Jelezko, J. R. Rabeau, N. Stavrias, A. D. Greentree, S. Prawer, J. Meijer, J. Twamley, P. R. Hemmer, and J. Wrachtrup, Nat. Phys. **2**, 408 (2006).
[33] S. T. van der, Z. Wang, M. Blok, H. Bernien, T. Taminiau, D. Toyli, D. Lidar, D. Awschalom, R. Hanson, and V. Dobrovitski, Nature (London) **484**, 82 (2012).
[34] M. Dutt, L. Childress, L. Jiang, E. Togan, J. Maze, F. Jelezko, A. Zibrov, P. Hemmer, and M. Lukin, Science **316**, 1312 (2007).
[35] P. B. Li, Z. L. Xiang, P. Rabl, and F. Nori, Phys. Rev. Lett. **117**, 015502 (2016).
[36] Z. Darázs, Z. Kurucz, O. Kálmán, T. Kiss, J. Fortágh, and P. Domokos, Phys. Rev. Lett. **112**, 133603 (2014).
[37] M. W. Doherty, F. Dolde, H. Fedder, F. Jelezko, J. Wrachtrup, N. B. Manson, and L. C. L. Hollenberg, Phys. Rev. B **85**, 205203 (2012).
[38] S. D. Bennett, N. Y. Yao, J. Otterbach, P. Zoller, P. Rabl, and M. D. Lukin, Phys. Rev. Lett. **110**, 156402 (2013).
[39] A. Jarmola, V. M. Acosta, K. Jensen, S. Chemerisov, and D. Budker, Phys. Rev. Lett. **108**, 197601 (2012).
[40] L. Childress and R. Hanson, MRS Bull. **38**, 134 (2013).
[41] M. G. Raymer, A. C. Funk, B. C. Sanders, and H. de Guise, Phys. Rev. A **67**, 052104 (2003).
[42] M. Kolář, T. Opatrný, and K. K. Das, Phys. Rev. A **92**, 043630 (2015).
[43] T. Opatrný, M. Kolář, and K. K. Das, Phys. Rev. A **91**, 053612 (2015).
[44] K. Ohashi, T. Rosskopf, H. Watanabe, M. Loretz, Y. Tao, R. Hauert, S. Tomizawa, T. Ishikawa, J. Ishi-Hayase, S. Shikata, C. L. Degen, and K. M. Itoh, Nano Lett. **13**, 4733 (2013).
[45] B. Grotz, M. V. Hauf, M. Dankerl, B. Naydenov, S. Pezzagna, J. Meijer, F. Jelezko, J. Wrachtrup, M. Stutzmann, F. Reinhard, and J. A. Garrido, Nat. Commun. **3**, 729 (2012).
[46] J. R. Weber, W. F. Koehl, J. B. Varley, A. Janotti, B. B. Buckley, C. G. Van de Walle, and D. D. Awschalom, Proc. Natl. Acad. Sci. USA **107**, 8513 (2010).
[47] W.-l. Song, Z.-q. Yin, W.-l. Yang, X.-b. Zhu, F. Zhou, and M. Feng, Sci. Rep. **5**, 7755 (2015).
[48] Y. Liu, J. You, and Q. Hou, Sci. Rep. **6**, 21775 (2016).
[49] H. Ian, Z. R. Gong, Y.-x. Liu, C. P. Sun, and F. Nori, Phys. Rev. A **78**, 013824 (2008).
[50] L. He, Y.-x. Liu, S. Yi, C. P. Sun, and F. Nori, Phys. Rev. A **75**, 063818 (2007).
[51] P. van Loock and A. Furusawa, Phys. Rev. A **67**, 052315 (2003).
[52] K. C. Lee *et al.*, Science **334**, 1253 (2011).